AGU PUBLICATIONS

Radio Science

RESEARCH ARTICLE
10.1002/2013RS005365

**Key Points:**
- A half-space may increase the link gain between small nodes
- Such a half-space may also bring no mismatch of the node antennas
- The results indicate an opportunity in the communication between small nodes

**Correspondence to:**
D. Penkin,
D.Penkin@tudelft.nl

**Citation:**
Penkin, D., G. Janssen, and A. Yarovoy (2014), Impact of a half-space interface on the wireless link between tiny sensor nodes, *Radio Sci.*, *49*, 798–811, doi:10.1002/2013RS005365.

Received 24 DEC 2013
Accepted 27 AUG 2014
Accepted article online 2 SEP 2014
Published online 29 SEP 2014

# Impact of a half-space interface on the wireless link between tiny sensor nodes

**Dmitriy Penkin[1], Gerard Janssen[2], and Alexander Yarovoy[1]**

[1]Microwave Sensing, Signals and Systems Group, Delft University of Technology, Delft, Netherlands, [2]Circuits and Systems Group, Delft University of Technology, Delft, Netherlands

**Abstract** The power budget of a wireless link between two electrically small sensor nodes located close to an interface between two media is studied. The model includes both the propagation channel losses and input impedance of the radio frequency antennas. It is shown that a highly inductive half-space significantly enhances the received power due to the contribution of the surface wave while not resulting in considerable mismatch losses between the antennas and electronics. Hence, such a half-space improves the link gain, which may compensate the limited energy available for transmission from electrically and physically small nodes.

## 1. Introduction

Advances in wireless communications and microelectromechanical systems technologies enable the development of networks with a large number of small and inexpensive sensor nodes. These networks nicknamed "Smart Dust" are foreseen to be a breakthrough technology which will enable a wide spectrum of emerging applications in environmental surveillance, civil engineering, and the health-care sector [*Ilyas and Mahgoub*, 2006; *Bush*, 2010]. Each individual sensor node integrates sensing, computing, and communication units to detect an environmental phenomenon and deliver the collected data to neighboring nodes (one-hop far away). By following a multihop communication paradigm, these data are forwarded throughout the network toward an end user.

As shown in *Akyildiz and Jornet* [2010], the most reliable way to establish a node-to-node connection in "Smart Dust" networks is based on electromagnetic (EM) waves. In practice, such wireless nodes will operate close to an interface between two media as it is important to tightly attach these sensors to it in order to avoid asbestos-like pathogenic effects on human beings who might breathe in the sensors [*Poland et al.*, 2008]. The impact of such an interface on the power budget of the node-to-node link might be substantial for the network realization: in particular, the existence of a strong link gain provoked by the interface is observed in *Zhang et al.* [2007], where the authors established a connection between microchips due to the surface wave contribution. The existence of a surface wave, excited by a vertical dipole over a lossy underlying half-space, and its properties were formulated and studied by Sommerfeld in his classic pioneering paper [*Sommerfeld*, 1909]. Several subsequent and independent researchers [e.g., *Wise*, 1931; *Norton*, 1936] have expanded his work. It was established that by increasing the communication distance, the surface wave amplitude diminishes slower than those of traditional spherical waves due to its cylindrical wavefront. The surface wave amplitude was, however, shown to decrease exponentially as the separation between the receiver and the surface increases. Thus, actual wireless links between two macroscale devices located close to an interface are typically modeled disregarding the surface wave impact because of such an electrically large separation. Conversely, as miniaturized nodes are located very close to the interface, the contribution of the surface wave to the received power cannot be neglected. To the best of our knowledge, the quantitative impact of the half-space, which supports a surface wave, on the wireless link between electrically small nodes is, however, not elucidated in the literature. In this paper, we develop the Green's function-based analytical model, capable of the quantitative evaluation of the interface impact on both the wireless propagation link and the characteristics of a node antenna. Using this model, we demonstrate the significance of the surface wave impact on the wireless propagation link in smart dust-like scenarios. Compared to the previously known solutions [*Li*, 2009; *King*, 1969; *Baños*, 1966], the developed model is implicitly improved by including in the link model the impact of electrically small transmitting and receiving antennas, current distribution, and input impedance, which are influenced by the interface.

To explore the impact of the surface wave on the link gain, we analyze first a two-layered half-space capable of supporting the surface wave. To rigorously determine this impact, we treat the problem using a full-wave method. Since the full-wave solution depends on the geometry of a particular half-space, we also propose a more general approach by employing the surface impedance $Z_s$ of the interface between upper and lower half-spaces. This impedance essentially simplifies the solution of the EM boundary value problem as there is no need to take care of the fields within the half-space. Eventually, numerical experiments are carried out to demonstrate that an underlying half-space, which supports a surface wave, concentrates EM energy in certain directions and can improve the link gain between two nodes due to the surface wave portion. Since this portion is very sensitive to the parameters of the underlying half-space, another point of interest is to formulate the criteria which should be imposed on the surface impedance to maximize the link gain.

Once the node antenna is placed very close to the interface, its input impedance will be affected by the interface resulting in mismatch losses between the antenna and transmitter. Evidently, such mismatch influences the power budget of the wireless link between two nodes. Hence, another objective of this work is to analyze such an input impedance as a function of the separation between the node antenna and the interface. Although this problem has attracted considerable attention in the past, the focus has primarily been either on further theoretical investigations of Sommerfeld's solution or developing approximate methods, which can satisfyingly model changes in the input impedance influenced by the half-space [*King et al.*, 1992; *Wait*, 1996; *Popovic and Djurdjevic*, 1995; *Michalski*, 1985; *Johnson and Dudley*, 1983; *King and Smith*, 1981; *Rudge*, 1972; *Vogler and Noble*, 1964; *Nicol and Ridd*, 1987]. Moreover, these methods typically addressed the input impedance of an antenna with a length of the order of a wavelength. Here the analytical model suitable to determine alterations in the input impedance of an electrically small antenna as a function of its separation from the interface is developed. Conditions under which mismatch losses between the antenna and transmitter have a negligible impact on the wireless power budget are found through numerical experiments.

The remainder of this paper is organized as follows: the system model is described in section 2. In section 3, the analytical model to obtain the received power over a two-layered half-space based on the full-wave formalism is developed, the way to treat it in a numerical fashion is thoroughly discussed, and numerical analysis is carried out. In section 4, the generalized model, which employs the impedance boundary condition, is developed and simulated. The impact of the interface on the input impedance of an electrically small antenna is modeled and numerically investigated in section 5. Finally, conclusions are drawn in section 6.

## 2. System Model

The geometry of the problem is depicted in Figure 1. The simple half-space supporting a surface wave includes an electrically thin dielectric layer coated on an ideal metal. The dielectric layer of thickness $d$ is lossy and characterized by a complex effective dielectric constant $\varepsilon$. The interfaces are regarded to be perfectly flat due to a short communication distance $R$. To maximize the impact of the surface wave on the wireless propagation link and thus its gain, the heights $z_t$ and $z_r$ are selected to be much smaller than the operating wavelength $\lambda$. Each sensor node is meanwhile equipped with an electrical dipole antenna to communicate and which is anchored to the half-space. Polarization of the dipole is supposed to be vertical as it is subject to considerably less attenuation than for horizontally polarized signals. The dipole length is equal to $l$, while its radius is $a$. Other sensor components are assumed to have no impact on the link budget. The cylindrical coordinates and $e^{j\omega t}$ time dependence are used throughout. Hence, the distance between two nodes along the $\rho$ axis is defined as $\rho$, whereas the distances between the interface and the center of the transmitting and receiving antenna are $z_t$ and $z_r$, respectively. The nodes are situated in the free half-space with parameters $\varepsilon_0 = (36\pi)^{-1} \times 10^{-9}$ F/m and $\mu_0 = 4\pi \times 10^{-7}$ H/m. The full-wave analysis involves a detailed treatment of EM fields within the half-space to obtain the Green's function, which is eventually used to estimate the received power based on the Hertz potential formalism. Thus, following *King and Smith* [1981], we assume that the current is triangularly distributed over the dipole. The analytical solution derived is represented through the Sommerfeld-type integral equation, which can formally be solved by applying the principle of stationary phase. However, this approach is limited to obtain the radiated field in the far field region of the antenna only. As the receiving antenna might be located in the near-field region of the

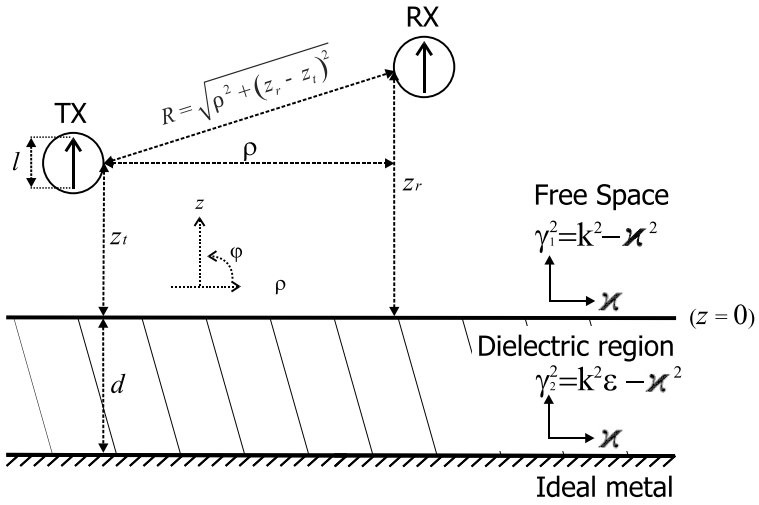


**Figure 1.** Problem geometry.

transmitting antenna due to severe constraints on the node energy source, the Sommerfeld-type solution is treated numerically. The technique in which an integration contour is deformed to a steepest descent path [*Parhami et al.*, 1980] is used to estimate the received power for any communication distance between two nodes.

For the impedance-based model, the interface is located along the plane $z = 0$ and incorporated in the model through a surface impedance $Z_s$. This parameter relates the electric $\vec{E}$ and magnetic fields $\vec{H}$ on its surface according to the Leontovich boundary condition $\hat{n} \times \vec{E} = Z_s \cdot \hat{n} \times (\hat{n} \times \vec{H})$, where $\hat{n}$ is the outward unit vector normal to the surface [*Senior and Volakis*, 1995]. Such a condition was originally proved to accurately treat any interface only when an incident plane wave comes from the zenith direction (incidence angle $\theta = 0$). However, the condition's applicability can be expanded to incident plane waves with any incidence angle once the half-space dielectric constant $\varepsilon \gg 1$: only in this case a charge density on the interface induced by a transmitting antenna is insensitive to its space position [*Godzinski*, 1961; *Senior and Volakis*, 1995]. According to *Vaynshteyn* [1969], the radius of the interface curvature $R_i$ should sufficiently exceed the communication distance $R$ to employ the Leontovich boundary condition in a safe manner. Therefore, to let EM fields at the receiving node, which are obtained using the impedance boundary condition, approximate accurately the exact fields, the impedance-based model is developed under the assumptions that $\varepsilon \gg 1$ and $R_i \gg R$. The received power is derived based on the Hertz potential formalism: in particular, the Green's function obtained by using $Z_s$ is utilized. The correctness of the impedance-based model is verified by comparing its results for the given two-layered half-space to those calculated using the full-wave approach.

To analyze the input impedance of the node antenna, the transmitting node is placed over the interface plane $z = 0$ with a surface impedance $Z_s$. The separation between the antenna and the interface is equal to $z_t$. Subsequently, both analytical and numerical treatments are similar to those developed and shown in section 3.

## 3. Two-Layered Half-Space

### 3.1. Analytical Model

As the node antenna is an electrically small dipole, its current distribution is approximated to be one-dimensional and triangularly distributed along the aperture [*King and Smith*, 1981]. The transmitting dipole is excited by a transmitter with frequency $f$ (wavelength $\lambda$) and amplitude $A$. To evaluate the pure interface impact on the node-to-node channel, the transmitter and receiver are considered to be perfectly matched to the antennas. Therefore, using the classical EM approaches [*Jackson*, 1962], a dominant

(with respect to the vertical polarization) electric field $E_z$ at the receiving point $(\rho, \varphi, z_r)$ is derived as follows:

$$E_z(\rho, z_r) = \left(\frac{\partial^2}{\partial z^2} + k^2\right)\Pi_z^e(\rho, \varphi, z_r) = \frac{-15AIi}{k}\left[\left(\frac{\partial^2}{\partial z^2} + k^2\right)G(\rho, z_r, 0, z_t)\right], \tag{1}$$

where $k = 2\pi/\lambda$ is the free-space wave number and $G(\rho, z_r, 0, z_t)$ corresponds to the Green's function for the vertical Hertz's dipole located above the given two-layered half-space. As the coordinate $\varphi$ does not influence the value $E_z$, the assumption $\varphi = \varphi_0 = 0$ is used without loss of generality and their notations are discarded throughout the rest of the paper. Based on the full-wave analysis, the function $G(\rho, z_r, 0, z_t)$ is formally derived in Appendix A and has the following form:

$$G(\rho, z_r, 0, z_t) = \int_{-\infty}^{\infty} \frac{\varkappa H_0^{(2)}(\varkappa\rho)\cdot e^{-i\gamma_1(z_r+z_t)}}{i\gamma_1\varepsilon + \gamma_2\tan(\gamma_2 d)}\mathrm{d}\varkappa, \tag{2}$$

where $\varkappa$ is the complex transverse wave number (Figure 1), while $\gamma_1^2 = k^2 - \varkappa^2$ and $\gamma_2^2 = k^2\varepsilon - \varkappa^2$ are the longitudinal wave numbers in free space and the dielectric region, respectively. As the current at the receiving antenna obeys the triangular distribution, the received power can thus be expressed mathematically using standard EM theory as follows:

$$p = \frac{I^2|E_z(\rho, z_r)|^2}{32\Re(Z_a)} = \frac{225A^2I^4}{32k^2\Re(Z_a)} \times \left|\left(\int_{-\infty}^{\infty} \frac{\varkappa^3 H_0^{(2)}(\varkappa\rho)\cdot e^{-i\gamma_1(z_r+z_t)}}{i\gamma_1\varepsilon + \gamma_2\tan(\gamma_2 d)}\mathrm{d}\varkappa\right)\right|^2, \tag{3}$$

where $I$ is the length and $Z_a$ the complex impedance of the antenna. Equation (3) contains the Sommerfeld-type integral, which has no formal solution. Such an integral can be treated using the stationary phase method [*King*, 1969] to produce an approximate analytical solution. The solution's applicability is, however, limited to cases where the receiver is in the far-field region of the transmitting antenna. To determine the received power at any communication distance, equation (3) is treated numerically. As it is intractable to evaluate the integral straightforwardly because of its highly oscillatory nature, the steepest descent path method [*Parhami et al.*, 1980] is applied in section 3.2. This method deforms the integration contour in order to simplify the procedure of obtaining the numerical integral solution.

### 3.2. Sommerfeld-Type Integral Treatment

To assure unique specification of the Sommerfeld-type integrand in equation (3) in the complex $\varkappa$ plane, it is necessary to discuss in detail the properties of the square root $\gamma_1 = \sqrt{k^2 - \varkappa^2}$. For $|\varkappa_i| < k$ the corresponding wave mode propagates along the $z$ axis, and its propagation constant $\gamma_{1i}$ should be real and positive. When $|\varkappa_i| > k$, to ensure that the radiated field in equation (3) remains limited with increasing the separation between a node and the interface as then $|\gamma_{1i}|\cdot|z_t + z_r| \to \infty$, the imaginary part of $\gamma_{1i}$ is required to be negative. Eventually, we need to impose the following restrictions:

$$\begin{cases} \gamma_1 > 0, \text{ when } |\varkappa| < k; \\ Im(\gamma_1) < 0, \text{ when } |\varkappa| > k. \end{cases} \tag{4}$$

To facilitate the solution process of the Sommerfeld-type integral, the complex variable $\xi$ is introduced through the transformation $\varkappa = k\cdot\sin\xi$, which changes equation (3) to equation (5).

$$p = \frac{225A^2I^4}{32k^2\Re(Z_a)} \times \left|\left(\int_{-\pi-i\infty}^{\pi+i\infty} \frac{k^3\sin^3(\xi)\cos(\xi)\cdot H_0^{(2)}(k\rho\sin(\xi))\cdot e^{-ik(z_t+z_r)\cos(\xi)}}{i\varepsilon\cos(\xi) + \sqrt{\varepsilon - \sin^2(\xi)}\cdot\tan\left(kd\sqrt{\varepsilon - \sin^2(\xi)}\right)}\mathrm{d}\xi\right)\right|^2. \tag{5}$$

$$p = \frac{225A^2I^4}{32k^2\Re(Z_a)} \times \left| \left( \int_{\overline{C}} \frac{k^3 \sin^3(\xi)\cos(\xi) \cdot H_0^{(2)}(k\rho\sin(\xi)) \cdot e^{-ik(z_t+z_r)\cos(\xi)}}{i\varepsilon\cos(\xi) + \sqrt{\varepsilon - \sin^2(\xi)} \cdot \tan\left(kd\sqrt{\varepsilon - \sin^2(\xi)}\right)} \mathrm{d}\xi \right. \right.$$

$$\left. \left. - \sum_{n=1}^{N} \frac{k^3 \sin^2(\xi_p^n)\cos(\xi_p^n) \cdot H_0^{(2)}(k\rho\sin(\xi_p^n)) \cdot e^{-ik(z_t+z_r)\cos(\xi_p^n)}}{i\varepsilon + \cos(\xi_p^n)\left[\frac{\cdot\tan\left(kd\sqrt{\varepsilon-\sin^2(\xi_p^n)}\right)}{\sqrt{\varepsilon-\sin^2(\xi_p^n)}} + \frac{kd}{\cos^2\left(kd\sqrt{\varepsilon-\sin^2(\xi_p^n)}\right)}\right]} \cdot \right) \right|^2 . \quad (6)$$

The complex $\varkappa$ plane is thus transformed into a single "$2\pi$-width" section of the complex $\xi$ plane due to the periodicity property $\sin(\xi + 2n\pi) = \sin\xi$ for $n = \pm1, \pm2, \ldots \pm \mathbb{N}$. Branch cuts, which are used on the two-sheeted complex Riemann $\varkappa$ plane to set the regulation of passing from one Riemann sheet to another to make the definition of the double-valued function $\gamma_1(\varkappa)$ unique, should be also mapped to the complex $\xi$ plane. In particular, the deformed integration contour $\overline{C}$ in the xi plane (Figure 2), which is introduced as according to *Felsen and Marcuvitz* [1994], meets the criteria for $\gamma_1$ postulated in equation (4). The continuous spectrum of eigenvalues $\xi \in \overline{C}$ corresponds to the spectrum of free-space modes with $\gamma_1 > 0$. The set of discrete points $\xi \in [\pi/2, \pi]$ describes surface wave modes [*Shevchenko*, 1971]. Note that although the poles of leaky wave modes are also determined through the simulations for quite thick dielectric layers, the leaky wave impact is seen to be negligible at the point receiver (the leaky wave contribution is quite restricted once the heights $z_t$ and $z_r$ are small and decays exponentially along the $\rho$ axis [*Felsen and Marcuvitz*, 1994]) and thus are neglected in this paper. Each surface mode propagates in the subsurface region (i.e., $\gamma_1^2 < 0$ and $\gamma_2^2 > 0$), and its pole $\xi_p$ has to be the root of the dispersive equation, which is basically the denominator of the integrand in equation (5). Hence, by obtaining the residues of these poles, the received power is decomposed as in equation (6). The first term in the brackets relates to the contribution of the geometric-optical wave. To determine the amount of received power caused by the portion of the surface wave, the sum in equation (6) should only be taken into account [*Shevchenko*, 1971].

### 3.3. Numerical Analysis

At first, by using equation (6) and following a geometric description of a numerical experiment conducted in *Li* [2009], the geometric-optical and surface wave field at the point receiver is calculated. Due to the nice agreement between the obtained results and those shown in Li's publication (see Figure 3), the full-wave model is endorsed. Moreover, although there is no straightforward mean to validate this model from a formal perspective, an indirect analytical support can still be provided by means of *Ling et al.* [1998]: the dispersion equation in this paper is similar to that derived here and being the denominator of the integrand in equation (5).

The analysis objective is to demonstrate that the impact of the simple two-layered half-space will substantially improve the link budget of the node-to-node channel under certain conditions. In particular, carbon is chosen as a reference dielectric material because it is low loss and widely used. Its dielectric properties have been characterized in *Hotta et al.* [2011], and $\varepsilon = 15 - 8i$ is particularly extracted at frequency $f = 10$ GHz. Calculations are performed for three different thicknesses: $d_1 = 5 \cdot 10^{-4}$ m, $d_2 = 10^{-3}$ m, and $d_3 = 10^{-2}$ m. The heights $z_t$ and $z_r$ are fixed to be equal to $\lambda/10$.

The dispersive equation is solved in a numerical manner as it is transcendent and unable to be analytically treated. In the course of its evaluation, the following is concluded: (1) a zero surface mode is always present in the dielectric layer, (2) the higher are the frequency $f$, the thickness $d$, and the dielectric constant $\varepsilon$, and the larger is the total number of surface modes, and (3) a multimode regime in the dielectric film occurs when $d > 2 \cdot 10^{-3}$ m. In particular, in Figure 4a a single root is estimated once the thickness is equal to $d_1$ or $d_2$. To demonstrate the significance of the interface impact, the power contribution of the surface wave $p_s$ is calculated for these thicknesses and normalized to that of the direct wave $p_{fs}$. Such a field strength is assessed using the free-space Green's function $e^{-ikR}/R$, where the communication distance $R$ is chosen to be

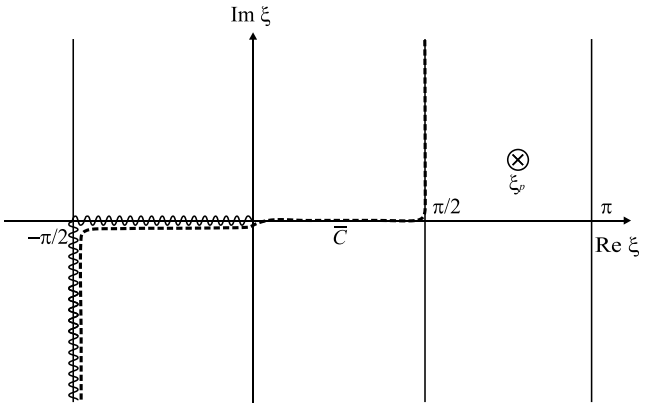


**Figure 2.** The integration contour $\bar{C}$ including the pole $\xi_p$.

the same as for calculating $p_s$. The link gain caused by the dielectric with thickness $d_1$ is shown to be larger than 10 dB when $R > 7\lambda$ (Figure 4b, dashed line). Meanwhile, the dielectric with thickness $d_2$ supports the surface wave, which increases the channel gain by more than 10 dB, once $2\lambda < R < 15\lambda$ (Figure 4b, short dashed line). Hence, the interface is shown through the numerical experiment to significantly influence the link gain of the node-to-node channel both at long and short communication ranges.

Now we will analyze the impact of the half-space, which allows multiple surface modes. In particular, the dielectric with thickness $d_3$ has four surface modes as its dispersive equation includes four different roots (Figure 4a). However, all these surface modes (including the zero one) convey a negligible amount of energy to the receiving node in free space: i.e., when $R = \lambda$, the ratio $p_s/p_{fs} = -51$ dB and reduces with increasing the communication range $R$. The same behavior is observed for the dielectric, which also supports the multiple surface modes but has a different thickness. Therefore, in the multimode scenario the surface wave will only propagate within the dielectric layer and produce negligible impact on the received signal in free space. In other words, the energy coupled into a dielectric slab of electrically large thickness (i.e., described by multiple modes) remains in the slab rather than propagating back to free space.

According to *Shevchenko* [1971], a half-space with a single-surface mode can be modeled in terms of its surface impedance. As the impedance-based model is attractive from a fundamental perspective since there is no need to take care of the fields within the underlying half-space, it is developed next.

## 4. Impedance Interface

### 4.1. Analytical Model

In this chapter we study the wireless link between two nodes over an interface in free space limited at $z = 0$ by the Leontovich boundary condition with surface impedance $Z_s$. The boundary condition as shown in *Senior and Volakis* [1995] can be used for modeling dielectric half-spaces with $\varepsilon \gg 1$ and is applicable to arbitrary incident angles. The received field is obtained by applying equation (1). The Green's function for a

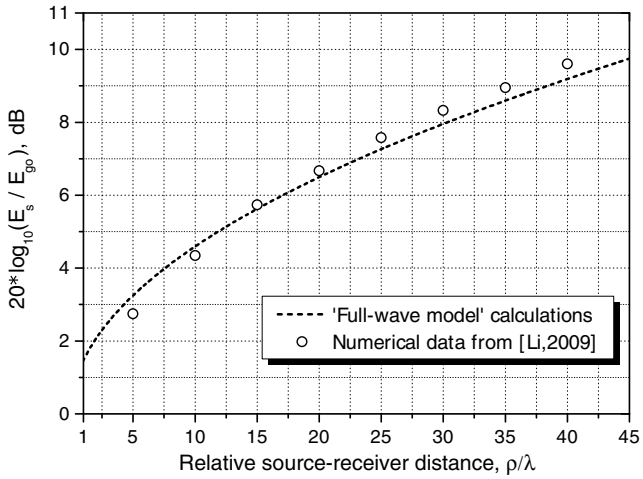


**Figure 3.** By using the full-wave model and following a geometric description of a numerical experiment conducted in *Li* [2009], the field strength of the surface wave normalized to that of the geometric-optical wave is calculated as a function of the source-receiver distance. The dots correspond to the data shown in Li's paper, Figure 2.11.

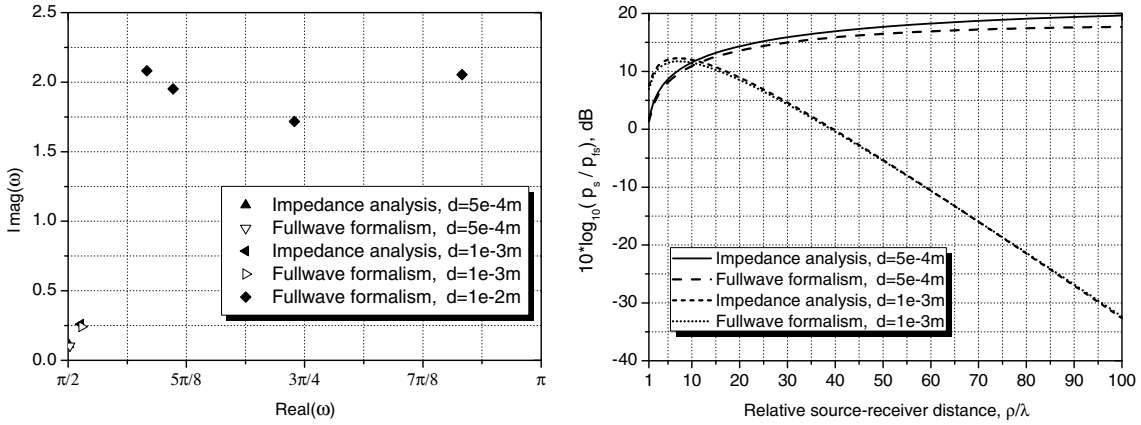


**Figure 4.** (a) The roots of dispersive equation $\xi_p$ are determined for the given values $d$. (b) The surface field strength normalized to that in the free space (the communication distance is the same for both scenarios) is demonstrated for the thicknesses $d_1$ and $d_2$.

vertical electric dipole situated over a flat interface with impedance $Z_s$ is derived from *Wait and Schlak* [1967] and given by equation (7).

$$G(\rho, z_r, 0, z_t) = \frac{e^{-ik\sqrt{\rho^2+(z_r-z_t)^2}}}{\sqrt{\rho^2+(z_r-z_t)^2}} + \int_{-\infty}^{\infty} \frac{\varkappa H_0^{(2)}(\varkappa\rho)}{\sqrt{\varkappa^2-k^2}} \cdot \frac{\sqrt{k^2-\varkappa^2}-k\overline{Z}_s}{\sqrt{k^2-\varkappa^2}+k\overline{Z}_s} \cdot e^{-i\sqrt{k^2-\varkappa^2}(z_r+z_t)} \mathrm{d}\varkappa. \tag{7}$$

$$p = \frac{225A^2I^4}{32k^2\Re(Z_a)} \times \left| \left( \left[\frac{\partial^2}{\partial z^2} + k^2\right] \frac{e^{-ik\sqrt{\rho^2+(z_t-z_r)^2}}}{\sqrt{\rho^2+(z_t-z_r)^2}} + \int_{\overline{C}} k^3 \sin^3(\xi) \cdot H_0^{(2)}(k\rho\sin(\xi)) \right.\right.$$
$$\left.\left. \cdot \frac{\cos(\xi)-\overline{Z}_s}{\cos(\xi)+\overline{Z}_s} \cdot e^{-ik\cos(\xi)(z_t+z_r)} \mathrm{d}\xi + 4\pi i \cdot k^3 \cdot (1-\overline{Z}_s^2) \cdot H_0^{(2)}\left(k\rho\sqrt{1-\overline{Z}_s^2}\right) \cdot \overline{Z}_s \cdot e^{ik(z_t+z_r)\overline{Z}_s} \right) \right|^2 . \tag{8}$$

The normalized surface impedance $\overline{Z}_s = Z_s/120\pi$. The first term in equation (7) corresponds to the free-space Green's function, while the second one represents the interface impact on the field at receiving point $(\rho, z_r)$. As $G(\rho, z_r, 0, z_t)$ contains the Sommerfeld-type integrand, the solution process is similar to that in section 3.2. Thus, the Green's function is revised using the transformation $\varkappa = k \cdot \sin\xi$. Since the restrictions on $\gamma_1$ are the same as in equation (4), the integration contour $\overline{C}$ is applied. Also, the residue of the unique pole $\xi_p = \arccos(-\overline{Z}_s)$ needs to be taken into account as it belongs to the proper Riemann sheet. Using equation (3), the power at the receiving node is eventually derived as in equation (8). Note that the power contribution of the direct, the reflected, and the surface wave can, respectively, be calculated by considering only the first, the second, and the third term in the round brackets of this equation.

To validate the impedance-based model, the given two-layered half-space is used and the obtained results are compared to those of the full-wave approach. The normalized surface impedance $\overline{Z}_s$ of the given half-space is derived by taking care of the boundary condition for EM fields on both surfaces of the dielectric layer and adopting the impedance boundary criterion at its upper interface and given by *Li* [2009]:

$$\overline{Z}_s = i(1/\varepsilon)^{1/2} \tan\left(k\sqrt{\varepsilon}d\right). \tag{9}$$

Once the dielectric thickness is equal to $d_1$ and $d_2$, the normalized impedances of the two-layered half-space are $\overline{Z}_s^1 = 0.0035 + 0.1107i$ and $\overline{Z}_s^2 = 0.0436 + 0.2635i$, respectively. For each thickness, the single root of the dispersive equation is seen in Figure 4a to be fairly approximated by $\xi_p = \arccos(-\overline{Z}_s)$, where $\overline{Z}_s$ is estimated using equation (9). In this way, the power contribution of the surface wave calculated by the impedance-based model for $z_t = z_r = \lambda/10$ is shown to be dominant and in good agreement with those obtained by the full-wave approach (Figure 4b). Such a nice match justifies the applicability of the impedance-based model to determine the interface impact on the power budget of the node-to-node channel.

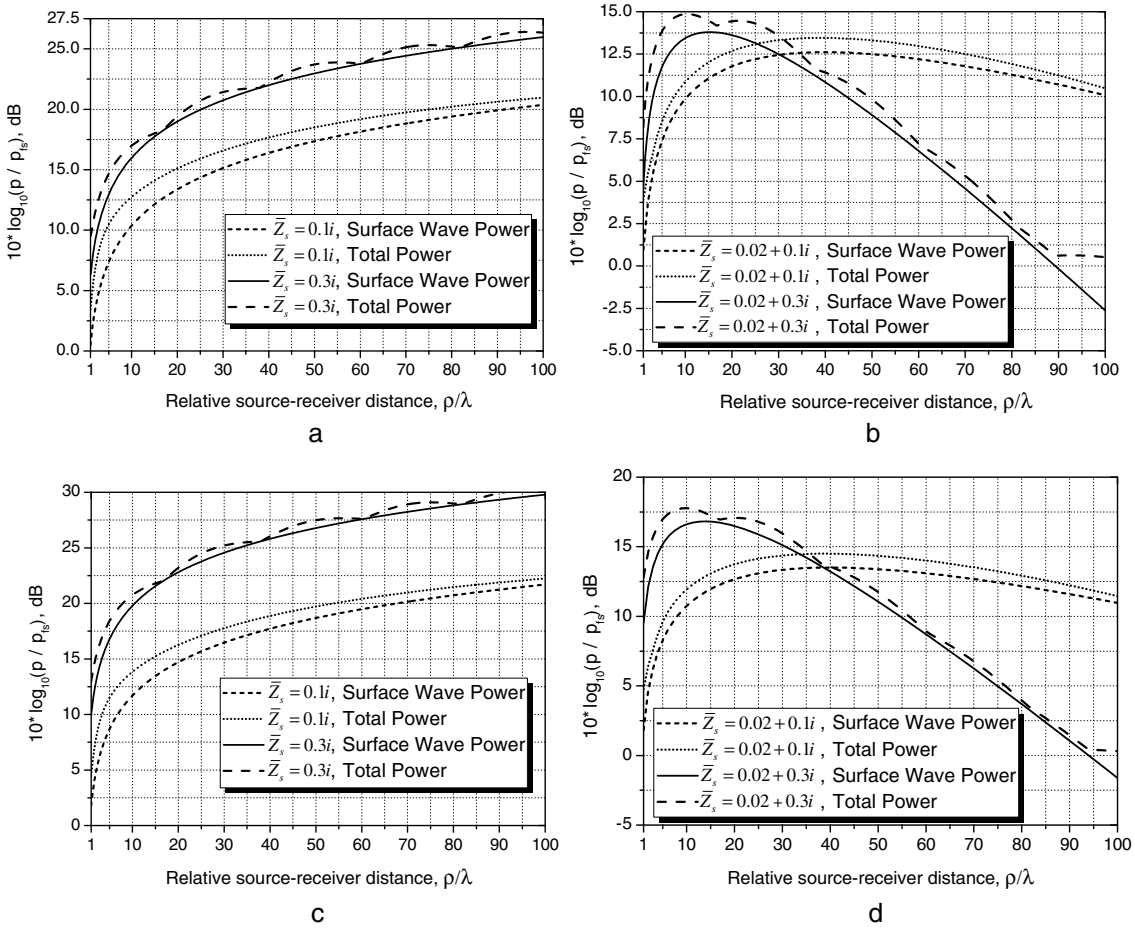


**Figure 5.** The total field power and its surface wave contribution as a function of the distance between the transmitting and receiving antennas. The obtained powers are normalized to the received power $p_{fs}$, which is related to a free-space wireless channel and calculated under the same conditions. (a and b) Plotted when $z_t = z_r = \lambda/10$. (c and d) Depicted for $z_t = z_r = \lambda/100$.

### 4.2. Numerical Analysis

The impact of the interface is investigated by comparing the total received power $p$ with a reference value $p_{fs}$, which corresponds to the power delivered through the free-space propagation channel. The power $p_{fs}$ is estimated by taking only into account the first term in the brackets of equation (8) as it represents the portion of the direct wave. To better understand the significance of the surface wave, the power contribution of this wave is assessed by solely considering the last term in the brackets of equation (8) in comparison with $p_{fs}$. The results, which are obtained for different values of $\overline{Z}_s$ as a function of the separation $z_t, z_r$, are shown in Figure 5. Note that the total power $p$ is calculated under the assumption that the surface wave constructively interferes with the geometric-optical counterpart as a phase shift between these waves is negligibly small due to a short communication range. In particular, the surface velocity has been demonstrated in Appendix C to be large enough to make this assumption. Also, the value of $\overline{Z}_s$ is considered to be limited as it is inversely proportional to the square root of the effective dielectric constant $\varepsilon$. Since $\varepsilon > 10$ to satisfy the impedance boundary condition criterion [*King*, 1969], the surface impedance is bounded as $\left|\overline{Z}_s\right| < 0.3$.

As can be seen in Figure 5, the interface impact depends significantly on its surface impedance. In particular, the larger is the positive imaginary part of $\overline{Z}_s$, and the better are the directive properties of the interface (i.e., no surface wave propagates above the half-space with a zero imaginary part). The losses of the underlying half-space are incorporated in the real part of $\overline{Z}_s$, and thus, the constructive impact from the interface is more significant when this real part tends to be zero. Eventually, once the half-space is described by a relatively high inductive impedance and the nodes are placed very close to it, the received power $p$ can be increased up to an order of magnitude compared to the "free-space" scenario due to the dominant contribution of the surface wave (Figures 5a and 5c). For example, once $\overline{Z}_s = 0.3i$ and $z_t = z_r = \lambda/100$, the link gain

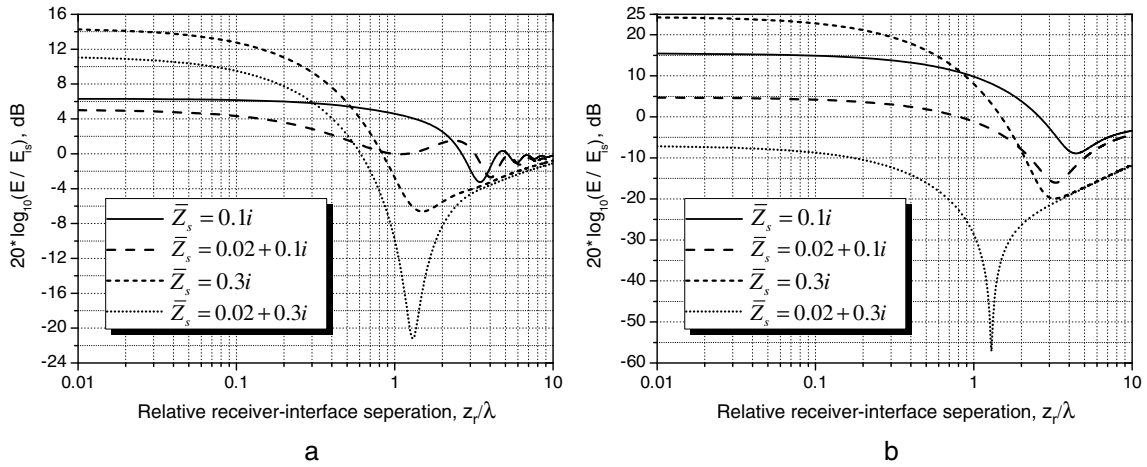


**Figure 6.** The field strength magnitude at the receiver $E$ influenced by the half-space with the impedance $\overline{Z}_s$ normalized to that $E_{is}$ affected by the perfectly conducting half-space $\overline{Z}_s = 0$ is demonstrated as a function of the receiver-interface separation $z_r$ when (a) $z_t = \lambda/10$, $\rho = 10\lambda$ and (b) $z_t = \lambda/10$, $\rho = 100\lambda$.

equals to 20 dB at $R = 10\lambda$ and its value increases with enlarging $R$. The existence of such a strong power gain may be explained by two facts: first, the surface wave field decays slower than the geometric-optical counterpart ($\sim 1/\sqrt{R}$ instead of $\sim 1/R$); second, a highly inductive half-space redistributes the EM fields by pulling them to the surface. The former is the well-known property of the surface wave coming from its cylindrical nature [*Vaynshteyn*, 1969]; meanwhile, the latter argument needs to be further investigated to prove its reliability. In particular, the EM field strength at the receiving node influenced by the half-space with the inductive impedance $\overline{Z}_s$ is compared to that affected by the perfectly conducting half-space ($\overline{Z}_s = 0$) in Figure 6. Since a perfectly conducting half-space produces a maximum geometric-optical portion as $R \gg \lambda$ and $z_t \ll \lambda$, such a comparison indicates how the geometric-optical field partly turns into a surface field as well as dissipated losses. In particular, its transformation into surface wave energy is seen from the trend that the field density increases for $z_r \ll \lambda$, whereas its magnitude decreases for larger $z_r$ (the half-space "attracts" the EM field to its surface). Meanwhile, for lossless half-spaces the magnitude of the EM field at $z_r \ll \lambda$ weakly decreases with increasing communication distance $R$ due to the slow decay of the surface wave (solid and short dashed lines in Figure 6). Once the half-space is lossy, despite of such a surface wave effect, the magnitude of the EM field at $z_r \ll \lambda$ may even reduce with increasing $R$ as the EM energy is partly dissipated (dashed and dotted curves in Figure 6).

## 5. Antenna Impedance

### 5.1. Analytical Model

The nearby interface influences the input impedance of the node antenna through changing its current distribution [*Rudge*, 1972]. For the modeling, the vertically polarized dipole is placed over the plane interface at height $z_t$. The antenna length is equal to $l \ll \lambda$, and its radius $a \ll l$. The half-space is characterized by the normalized surface impedance $\overline{Z}_s$.

The dipole impedance is analytically derived in Appendix B. This impedance can be decomposed as $Z_a = Z_{fs} + \Delta Z$, where $Z_{fs}$ is the input impedance of the antenna in free space and $\Delta Z$ is the change due to the presence of the half-space. The free-space antenna impedance $Z_{fs}$ has been determined in *King and Smith* [1981]. Being the measure of the interface impact, the value $\Delta Z$ includes the Sommerfeld-type integrand and is revised using the transformation $\varkappa = k \cdot \sin(\xi)$ and given by equation (10). This equation is treated in a similar fashion as before, and the final form of $\Delta Z$ is derived as in equation (11).

$$\Delta Z = \frac{15 I^2 k^2}{2} \int_{-\pi - i\infty}^{\pi + i\infty} \sin^3(\xi) \cdot H_0^{(2)}(k\rho \sin(\xi)) \cdot \frac{\cos(\xi) - \overline{Z}_s}{\cos(\xi) + \overline{Z}_s} \cdot e^{-2ikz_t \cos(\xi)} d\varkappa. \tag{10}$$

$$\Delta Z = \frac{15l^2k^2}{2}\left[\int_{\overline{C}} \sin^3(\xi)\cdot H_0^{(2)}(k\rho\sin(\xi))\cdot\frac{\cos(\xi)-\overline{Z}_s}{\cos(\xi)+\overline{Z}_s}\cdot e^{-2ikz_t\cos(\xi)}\mathrm{d}\varkappa\right.$$
$$\left. + 4\pi i\cdot \left(1-\overline{Z}_s^2\right)\cdot H_0^{(2)}\left(k\rho\sqrt{1-\overline{Z}_s^2}\right)\cdot\overline{Z}_s\cdot e^{2ikz_t\overline{Z}_s}\right]. \quad (11)$$

### 5.2. Numerical Analysis

To address $\Delta Z$ as a function of the normalized surface impedance $\overline{Z}_s$, the parameters of the radiating dipole are fixed to be $l = 0.01\lambda$ and $a = 0.01l$, where $\lambda = 3\cdot 10^{-2}$ m. The impedance of such a dipole in free space is estimated to be $Z_{fs} = 0.019 - 11596i$ Ohm. Meanwhile, the complex value $\Delta Z$ is shown as a function of the separation $z_t$ in Figure 7 for several interfaces characterized by $\overline{Z}_s = 0$, $\overline{Z}_s = 0.1i$, and $\overline{Z}_s = 0.25i$, respectively. It can be seen that the obtained results match those calculated using the electromagnetic solver *FEKO* [1994]. The latter could be assessed in the following way. First, the dipole antenna in free space is modeled in *FEKO* [1994] as a one-dimensional wire element with the feed point at the middle and its impedance $Z_{fs}$ is straightforwardly determined via simulations. Second, the antenna impedance $Z_a$ is directly estimated by *FEKO* [1994] considering the same dipole antenna over a planar two-layered substrate. Both thickness and dielectric permittivity of layers are selected to provide the interface along the plane $z = 0$ with the required impedance $\overline{Z}_s$ according to equation (9) (excluding the interface characterized by $\overline{Z}_s = 0$, which stands for the half-space made of a perfectly conducting metal). Finally, for each set of input parameters the complex value $\Delta Z$ is assessed by subtracting $Z_{fs}$ from $Z_a$.

As a transmitter can typically adapt the real part of its impedance to avoid a mismatch with the antenna, the attention is primarily paid to the imaginary part of $Z_a$. It can be concluded from Figure 7 that the rate of increase of the imaginary part $\Im(\Delta Z)$ grows with lowering the value $\overline{Z}_s$. This finding is explained by the fact that with decreasing $\overline{Z}_s$ the interface tends to behave as a perfect conductor, which is known to strongly affect only the imaginary part of a vertically polarized antenna. Meanwhile, the starting point of increasing $\Im(\Delta Z)$ is independent from the properties of an underlying half-space. While modeling the transmitting antenna of a different length and radius, it appears that such a starting point is mainly related to the ratio $z_t/l$. From a physical perspective, it can be explained that the separation between the antenna and interface $z_t$ has to be increased in order to not induce a perturbation of currents on the aperture of a larger antenna. Our results suggest that the value $\Im(\Delta Z)$ can be considered insignificant once $z_t/l \geqslant 1$ for any kind of half-space and antenna radius $a \leqslant 0.1l$. Hence, once the separation $z_t$ exceeds the dipole length $l$, the interface will cause a negligible mismatch between the antenna and transmitter as it does not affect the imaginary part of $Z_a$. Moreover, the real part $\Re(\Delta Z)$, which is directly associated with the amount of energy radiated from the antenna, can even be enhanced by means of the nearby interface (Figure 7).

## 6. Conclusion

To analyze the impact of a media interface on the wireless link between two nodes of a smart dust-like network, we have developed analytical models to describe the impact of this interface both on the propagation path and the node antennas and performed numerical analysis. We assumed that each node is equipped with an electrically small vertically polarized linear dipole. The transmitting and receiving nodes are placed over the half-space at heights $z_t$ and $z_r$, respectively, much smaller than the operating wavelength.

First, the influence of the surface wave existing in a two-layered half-space on the node-to-node channel has been modeled using the full-wave analysis. Through numerical experiments, it has been shown that particular realizations of this half-space have a constructive and significant influence on the power budget of such a wireless link: once the communication distance $R > 2\lambda$ and $z_t = z_r = \lambda/10$, the link gain has been shown to increase by more than 10 dB due to the contribution of the surface wave. It has been shown that a two-layered medium can fairly be treated using the surface impedance concept. Hence, the impedance-based model has been developed to describe the impact of a generic interface on a wireless link. Such a model is attractive from a fundamental perspective as there is no need to take care of the fields within the half-space. The model has been verified by comparison with available full-wave simulation results in particular cases. The subsequent numerical analysis demonstrates that a half-space

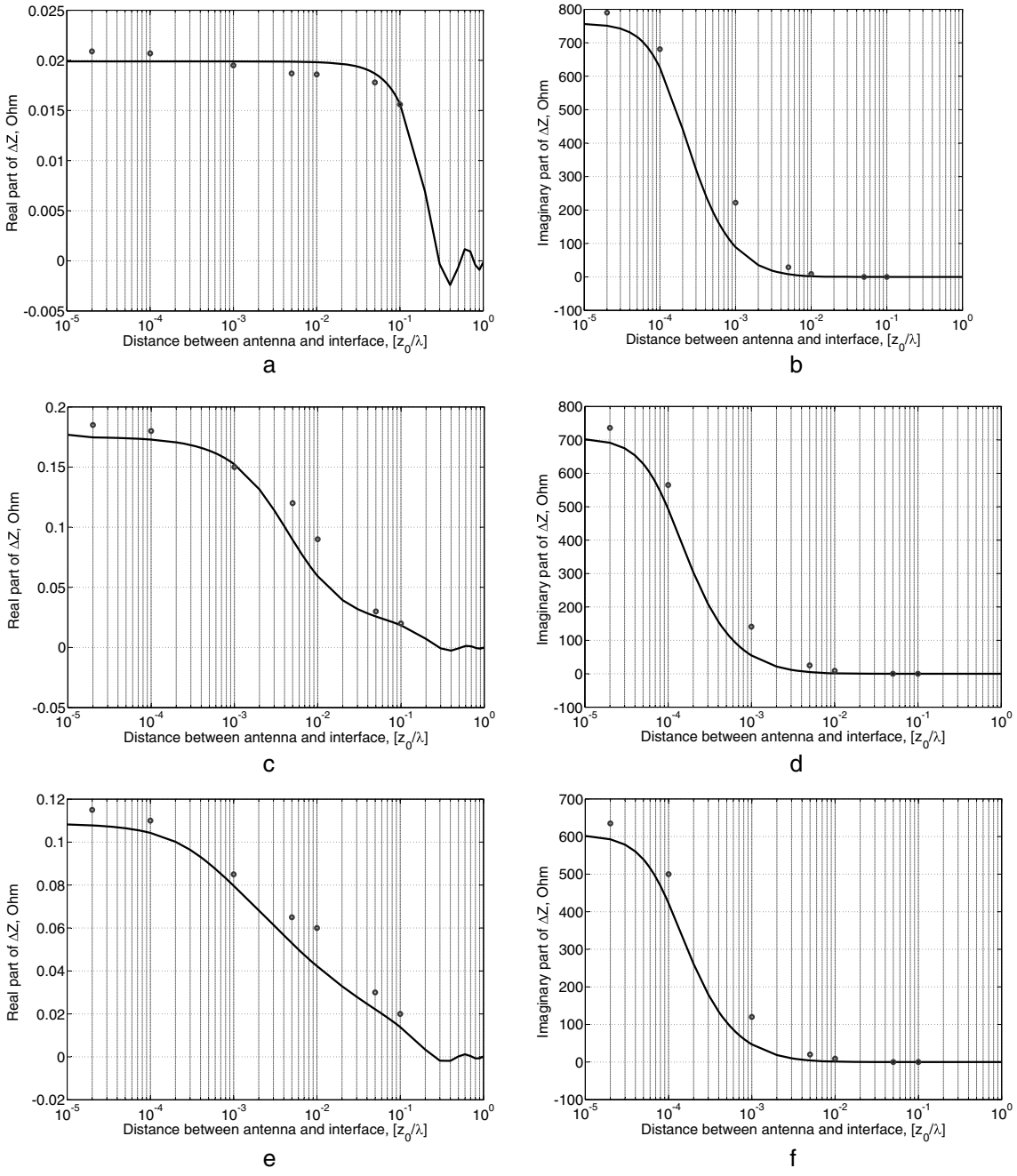


**Figure 7.** The value of $\Delta R$ for different types of half-space: (a and b) $Z_s = 0$, (c and d) $Z_s = 0.1i$, (e and f) $Z_s = 0.25i$. The results obtained are shown in solid line, while those simulated in *FEKO* [1994] are depicted by markers.

with a highly inductive impedance substantially improves the power budget of the node-to-node link: i.e., the link gain increase is more than 20 dB when $R > 10\lambda$ and $z_t = z_r = \lambda/100$. The existence of such a large gain is explained by two facts: (1) the surface wave field decays slower than the geometric-optical counterpart ($\sim 1/\sqrt{R}$ instead of $\sim 1/R$) and (2) a highly inductive half-space redistributes the EM fields by pulling them to the surface. From the node design point of view, this finding suggests developing antennas which will mainly transfer transmitting power in a surface wave rather than in space (volumetric) wave.

Second, the influence of the nearby half-space on the antenna impedance has analytically been studied since it might cause a mismatch between the node antenna and transmitter. Numerical simulations have

shown that the half-space negligibly affects the antenna input impedance once the separation $z_t$ between antenna and interface exceeds the dipole length $l$.

Our analysis shows that the half-space characterized by a highly inductive impedance significantly and constructively affects the wireless path gain between miniaturized nodes without bringing extra mismatch of the node antennas (the criteria $z_t > l, z_r > l$ must be fulfilled). This finding is essential from a practical perspective as it offers an opportunity to communicate between miniaturized electronic devices: i.e., thanks to the strong link gain provoked by such an interface, the wireless link between nodes with electrically smaller antenna is realizable, and thus, a more functional wireless sensor network can be implemented. Unlike the perfectly conducting half-space which merely supports the geometric-optical wave (it is formed as an interference of direct and reflected waves, and thus, its magnitude is subject to substantial alterations with varying source-receiver distance), the interface with a highly inductive surface impedance is moreover capable of maintaining the wireless link over a wide and continuous range of communication distances due to the significant contribution of the surface wave.

## Appendix A: Green's Function of a Vertical Dipole Located Over a Two-Layered Half-Space

Here the Green's function of a vertically polarized elemental dipole located over the given two-layered half-space is derived. As shown in Figure 1, the dipole is placed in the point $(0, 0, z_t)$. The general representation of the Green's function $G(\rho, z_r, 0, z_t)$ for a vertical elemental antenna located over an interface is known to be written as [*Felsen and Marcuvitz*, 1994]

$$G(\rho, z_r, 0, z_t) = \frac{1}{4\pi} \int_{-\infty}^{\infty} \varkappa H_0^{(2)}(\varkappa\rho) g(z_r, z_t) \mathrm{d}\varkappa, \tag{A1}$$

where $\varkappa$ is the complex transverse wave number, $H_0^{(2)}$ stands for the Hankel function of the second kind, and zero order and the function $g(z_r, z_t)$ is the one-dimensional modal Green's function. The function $g(z_r, z_t)$ depends generally on the nature of $z$ stratification. For the given half-space, $g(z_r, z_t)$ is derived by adopting the rigorous boundary conditions (e.g., the tangential components of the electric field are continuous across the interface) on both surfaces of the dielectric layer and by using the wave equations for free space and the dielectric medium. This results in a system of four linear equations with four unknown parameters. By solving it, the representation of $g(z_r, z_t)$ is expressed as follows:

$$g(z_r, z_t) = \frac{4\pi \cdot e^{-i\gamma_1(z_r+z_t)}}{i\gamma_1\varepsilon + \gamma_2 \tan(\gamma_2 d)}, \tag{A2}$$

where $\gamma_1^2 = k^2 - \varkappa^2$ and $\gamma_2^2 = k^2\varepsilon - \varkappa^2$ are the longitudinal wave numbers in free space and the dielectric region, respectively. In this way, the final form of the Green's function $G(\rho, z_r, 0, z_t)$ is given by

$$G(\rho, z_r, 0, z_t) = \int_{-\infty}^{\infty} \frac{\varkappa H_0^{(2)}(\varkappa\rho) \cdot e^{-i\gamma_1(z_r+z_t)}}{i\gamma_1\varepsilon + \gamma_2 \tan(\gamma_2 d)} \mathrm{d}\varkappa. \tag{A3}$$

## Appendix B: Input Impedance of a Vertical Dipole Placed Over an Impedance Half-Space

Here the input impedance of a vertical dipole located over the impedance interface at height $z_t$ is derived. The dipole length is equal to $l \ll \lambda$, while $a \ll l$ stands for its radius. The interface is characterized by the normalized surface impedance $\overline{Z}_s$.

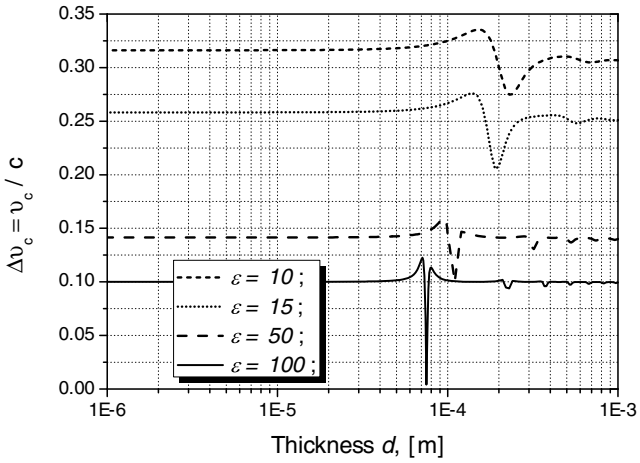


**Figure C1.** The value $\Delta v_c = \frac{v_c}{c}$ as a function of thickness $d$ for various types of the two-layered half-spaces ($v_c$ is the group velocity of the surface wave).

The antenna is modeled to be fed through a delta voltage generator located at its center. Hence, the dipole is excited with the following signal:

$$E_z(a,z) = -V_0 \cdot \delta(z - z_t), \tag{B1}$$

where $V_0$ is the amplitude [V]. By taking into account that $V_0 = Z_a \cdot j(z_r)$ and using equations (1), (7), and standard mathematical methods, the above expression can be written as equation (B2). The first term in the square brackets corresponds to the free-space Green's function, while the second term includes the interface impact. Therefore, the antenna impedance $Z_a$ can be decomposed as $Z_a = Z_{fs} + \Delta Z$, where $Z_{fs}$ is the impedance of the dipole in free space and $\Delta Z$ is the portion due to the presence of the half-space. Through simple algebra, the value of $\Delta Z$ is determined as in equation (B3).

$$Z_a = \frac{30i}{k} \cdot \int_{z_t - l/2}^{z_t + l/2} \left(1 - \frac{|z - z_t|}{l/2}\right) \cdot \left[\frac{\partial^2}{\partial z^2} + k^2\right] \int_{z_t - l/2}^{z_t + l/2} \left(1 - \frac{|z' - z_t|}{l/2}\right) \left[\frac{e^{-ik\sqrt{\rho^2 + (z-z')^2}}}{\sqrt{\rho^2 + (z-z')^2}} + \int_{-\infty}^{\infty} \frac{\varkappa H_0^{(2)}(\varkappa\rho)}{i\sqrt{k^2 - \varkappa^2}} \cdot \frac{\sqrt{k^2 - \varkappa^2} - k\overline{Z}_s}{\sqrt{k^2 - \varkappa^2} + k\overline{Z}_s} \cdot e^{-i\sqrt{k^2 - \varkappa^2}(z+z')} \mathrm{d}\varkappa\right] \mathrm{d}z' \, \mathrm{d}z. \tag{B2}$$

$$\Delta Z = \frac{15l^2}{2k} \int_{-\infty}^{\infty} \frac{\varkappa^3 H_0^{(2)}(\varkappa\rho)}{\sqrt{k^2 - \varkappa^2}} \cdot \frac{\sqrt{k^2 - \varkappa^2} - k\overline{Z}_s}{\sqrt{k^2 - \varkappa^2} + k\overline{Z}_s} \cdot e^{-2iz_t\sqrt{k^2 - \varkappa^2}} \mathrm{d}\varkappa. \tag{B3}$$

## Appendix C: Velocity of a Surface Wave in a Two-Layered Half-Space

According to *Vaynshteyn* [1969], the group velocity of the surface wave $v_c$ is given by

$$v_c = v \cdot \Re(\varkappa_p), \tag{C1}$$

where $v$ is the wave propagation velocity in the dielectric, whereas $\varkappa_p$ is the transverse wave number of the surface wave. The wave propagation velocity is known to be expressed as

$$v = \frac{c}{\sqrt{\Re(\varepsilon)}}, \tag{C2}$$

where $c$ is the speed of light and $\varepsilon$ is the dielectric constant of the upper half-space layer. The transverse wave number can be derived through the surface impedance as $\varkappa_p = \sqrt{1 - \overline{Z}_s^2}$. Hence, using equations (C1) and (C2), the ratio $\Delta v_c = v_c/c$ can be given as

$$\Delta v_c = \frac{\Re\left(\sqrt{1 - \overline{Z}_s^2}\right)}{\sqrt{\Re(\varepsilon)}}. \tag{C3}$$

For the given two-layered half-space, the ratio $\Delta v_c = v_c/c$ is plotted in Figure C1 as a function of the thickness $d$ at the wavelength $\lambda = 0.03$ m. Note that the dielectric constant $\varepsilon$ is selected both actual and hypothetical to better understand its influence on the group velocity $v_c$. The numerical results indicate that $v_c \ll c$ only when $\Re(\varepsilon) \geqslant 100$. However, the most constructive impact on the power budget of the

node-to-node channel is expected once the half-space has a high inductive impedance and is thus characterized by a low value of $\Re(\epsilon)$. Hence, due to $v_c \sim c$ and the small communication distance, the assumption that there is no phase shift between the surface and the geometric-optical waves is valid.

**Acknowledgments**
The authors thank the anonymous reviewers for their constructive and helpful comments.

## References

Akyildiz, I., and J. Jornet (2010), Electromagnetic wireless nanosensor networks, *Nano Commun. Networks*, *1*(1), 3–19.
Baños, A. (1966), *Dipole Radiation in the Presence of a Conducting Half-Space*, International Series of Monographs in Electromagnetic Waves, Pergamon Press, Oxford.
Bush, S. F. (2010), *Nanoscale Communication Networks*, Artech House, Norwood.
FEKO (1994), *Computational Electromagnetics Software*. [Available at http://www.feko.info/.]
Felsen, L., and N. Marcuvitz (1994), *Radiation and Scattering of Waves*, IEEE Press Series on Electromagnetic Wave Theory, Wiley, N. J.
Godzinski, Z. (1961), The surface impedance concept and the structure of radio waves over real earth, *Proc. IEEE*, *108*(14), 362–373.
Hotta, M., M. Hayashi, M. Lanagan, D. Agrawal, and K. Nagata (2011), Complex permittivity of graphite, carbon black and coal powders in the ranges of X-band frequencies (8.2 to 12.4 GHz) and between 1 and 10 GHz, *ISIJ Int.*, *51*(11), 1766–1772.
Ilyas, M., and I. Mahgoub (2006), *Smart Dust: Sensor Network Applications, Architecture and Design*, CRC Press, Boca Raton, Fla.
Jackson, J. D. (1962), *Classical Electrodynamics*, vol. 3, Wiley, New York.
Johnson, W. A., and D. G. Dudley (1983), Real axis integration of Sommerfeld integrals: Source and observation points in air, *Radio Sci.*, *18*(2), 175–186.
King, R., and G. Smith (1981), *Antennas in Matter: Fundamentals, Theory and Applications*, Mit Press, Cambridge, Mass.
King, R., M. Owens, and T. Wu (1992), *Lateral Electromagnetic Waves: Theory and Applications to Communications, Geophysical Exploration, and Remote Sensing*, Graduate Texts in Contemporary Physics, Springer, New York.
King, R. J. (1969), Electromagnetic wave propagation over a constant impedance plane, *Radio Sci.*, *4*(3), 255–268.
Li, K. (2009), *Electromagnetic Fields in Stratified Media*, Advanced Topics in Science and Technology in China, Springer, Berlin Heidelberg.
Ling, R., J. Scholler, and P. Y. Ufimtsev (1998), The propagation and excitation of surface waves in an absorbing layer, *Progr. Electromagnet. Res.*, *19*, 49–91.
Michalski, K. (1985), On the efficient evaluation of integral arising in the Sommerfeld half space problem, *IEE Proc. H Microwaves Antennas Propag.*, *132*(5), 312–318.
Nicol, J., and P. Ridd (1987), *Antenna Input Impedance: Experimental Confirmation and Geological Application*, Natural Philosophy Research Report Series, James Cook Univ., Townsville, North Queensland, Australia.
Norton, K. (1936), The propagation of radio waves over the surface of the earth and in the upper atmosphere, *Proc. Inst. Radio Eng.*, *24*(10), 1367–1387.
Parhami, P., Y. Rahmat-Samii, and R. Mittra (1980), An efficient approach for evaluating Sommerfeld integrals encountered in the problem of a current element radiating over lossy ground, *IEEE Trans. Antennas Propag.*, *28*(1), 100–104.
Poland, C. A., R. Duffin, I. Kinloch, A. Maynard, W. A. H. Wallace, A. Seaton, V. Stone, and S. Brown (2008), Carbon nanotubes introduced into the abdominal cavity of mice show asbestos-like pathogenicity in a pilot study, *Nat. Nanotechnol.*, *3*, 423–428.
Popovic, B., and D. Djurdjevic (1995), Entire-domain analysis of thin-wire antennas near or in lossy ground, *IEE Proc. Microwaves Antennas Propag.*, *142*(3), 213–219.
Rudge, A. (1972), Input impedance of a dipole antenna above a conducting half space, *IEEE Trans. Antennas Propag.*, *20*(1), 86–89.
Senior, T. B., and J. L. Volakis (1995), *Approximate Boundary Conditions in Electromagnetics*, vol. 41, IET, London.
Shevchenko, V. (1971), *Continuous Transitions in Open Waveguides: Introduction to the Theory*, The Golem Series in Electromagnetics, Golem Press, Boulder, Colo.
Sommerfeld, A. (1909), Über die ausbreitung der wellen in der drahtlosen telegraphie [On the propagation of waves for the wireless telegraphy], *Ann. Phys. Leipzig*, *28*, 665–737.
Vaynshteyn, L. A. (1969), *Open Resonators and Open Waveguides*, Golem Press, Boulder, Colo.
Vogler, L., and J. Noble (1964), *Curves of Input Impedance Change Due To Ground for Dipole Antennas*, pp. 72–79, Monograph, National Bureau of Standards, United States.
Wait, J. (1996), *Electromagnetic Waves in Stratified Media*, The IEEE/OUP Series on Electromagnetic Wave Theory / Donald G. Dudley, Institute of Electrical and Electronic Engineers, New York.
Wait, J., and G. Schlak (1967), New asymptotic solution for the electromagnetic fields of a dipole over a stratified medium, *Electron. Lett.*, *3*(9), 421–422.
Wise, W. H. (1931), The grounded condenser antenna radiation formula, *Proc. Inst. Radio Eng.*, *19*(9), 1684–1689.
Zhang, Y. P., Z. M. Chen, and M. Sun (2007), Propagation mechanisms of radio waves over intra-chip channels with integrated antennas: Frequency-domain measurements and time-domain analysis, *IEEE Trans. Antennas Propag.*, *55*(10), 2900–2906.